

ARTICLE

Received 3 Apr 2013 | Accepted 23 Sep 2013 | Published 24 Oct 2013

DOI: 10.1038/ncomms3658

# Polycystin-1 binds Par3/aPKC and controls convergent extension during renal tubular morphogenesis

Maddalena Castelli<sup>1,2</sup>, Manila Boca<sup>1</sup>, Marco Chiaravalli<sup>1</sup>, Harini Ramalingam<sup>3,4</sup>, Isaline Rowe<sup>1</sup>, Gianfranco Distefano<sup>1</sup>, Thomas Carroll<sup>3,4</sup> & Alessandra Boletta<sup>1</sup>

Several organs, including the lungs and kidneys, are formed by epithelial tubes whose proper morphogenesis ensures correct function. This is best exemplified by the kidney, where defective establishment or maintenance of tubular diameter results in polycystic kidney disease, a common genetic disorder. Most polycystic kidney disease cases result from loss-of-function mutations in the *PKD1* gene, encoding Polycystin-1, a large receptor of unknown function. Here we demonstrate that PC-1 has an essential role in the establishment of correct tubular diameter during nephron development. Polycystin-1 associates with Par3 favouring the assembly of a pro-polarizing Par3/aPKC complex and it regulates a programme of cell polarity important for oriented cell migration and for a convergent extension-like process during tubular morphogenesis. Par3 inactivation in the developing kidney results in defective convergent extension and tubular morphogenesis, and in renal cyst formation. Our data define Polycystin-1 as central to cell polarization and to epithelial tube morphogenesis and homeostasis.

<sup>1</sup>Division of Genetics and Cell Biology, Dulbecco Telethon Institute (DTI) at DIBIT, San Raffaele Scientific Institute, Via Olgettina, 58, 20132 Milan, Italy. <sup>2</sup>Ph.D. Program in Molecular and Cellular Biology, Vita-Salute San Raffaele University, Via Olgettina, 58, 20132 Milan, Italy. <sup>3</sup>Division of Nephrology, Department of Internal Medicine, University of Texas Southwestern Medical Center, 5323 Harry Hines Boulevard, NA8 124, Dallas, Texas 75390-9148 USA. <sup>4</sup>Department of Molecular Biology, University of Texas Southwestern Medical Center, 5323 Harry Hines Boulevard, NA8 124, Dallas, Texas 75390-9148 USA. Correspondence and requests for materials should be addressed to A.B. (email: boletta.alessandra@hsr.it).

The kidney develops as a result of interactions between the ureteric bud (UB) and the metanephric mesenchyme (MM)<sup>1</sup>. The UB invades the MM and undergoes a series of branchings forming the collecting duct system and ureter of the mature kidney<sup>1</sup>. The UB also induces a condensation and epithelialization of the MM to form comma and S-shaped bodies. The mechanisms responsible for UB branching and MM condensation have been thoroughly studied over the years with important progress being made<sup>1</sup>. By contrast, the mechanisms responsible for the subsequent steps of maturation have been the focus of more recent studies, and many outstanding questions remain<sup>1</sup>. Comma and S-shaped bodies are composed of an immature epithelium with a central lumen, which will undergo a programme of patterning. Both MM- and UB-derived structures undergo a programme of tubular elongation necessary to generate the mature nephron and collecting duct system, respectively<sup>2</sup>.

Recent important progress has been made in understanding the mechanisms underlying the elongation process, as well as the establishment and maintenance of tubular diameter<sup>1–3</sup>. This process is achieved by at least two mechanisms. During embryonic development, both the collecting duct and the proximal tubules decrease in diameter. Although cell division is randomly oriented at these stages, tubular elongation involves a process similar to convergent extension (CE) movements, which are known to cause narrowing and elongation of tissues in several systems<sup>1</sup>. It was recently shown that epithelial cells

composing the tubules achieve a precise orientation and elongate mediolaterally, in a process resulting in cellular intercalation<sup>3,4</sup>. This process depends on the planar cell polarity pathway (PCP) and involves the formation and resolution of rosettes, in a process closely resembling CE<sup>3</sup>. Once this initial phase of morphogenesis is completed (approximately at postnatal day 1 in most collecting ducts in the mouse) and the optimal tubular diameter is reached, further elongation of the tubule is achieved by oriented (proximal–distal) cell division (OCD)<sup>4,5</sup>, ensuring elongation, while preserving a correct diameter. Defects in the PCP pathway altering one or both of these processes have been proposed to contribute to cystogenesis<sup>4,5</sup>.

Defective regulation of tubular diameter is associated with autosomal dominant polycystic kidney disease (PKD), one of the most common inherited disorders<sup>6</sup>. The hallmark of this disease is bilateral renal cyst formation, due to loss-of-function mutations in two genes: *PKD1* in 85% of cases or *PKD2* in the remaining 15%. Expression of the *PKD1* gene is developmentally regulated in the kidneys<sup>7</sup>, suggesting its possible involvement in normal tubular morphogenesis. *PKD1* encodes for Polycystin-1 (PC-1), a large plasma membrane receptor of unknown function, with a very large extracellular amino terminus containing protein–protein interaction domains, 11 transmembrane domains and a short intracellular carboxy terminus<sup>7</sup>. PC-1 has been implicated in a number of biological processes<sup>7</sup>, but to date its precise function remains to be defined. The role of the *Pkd1* gene in

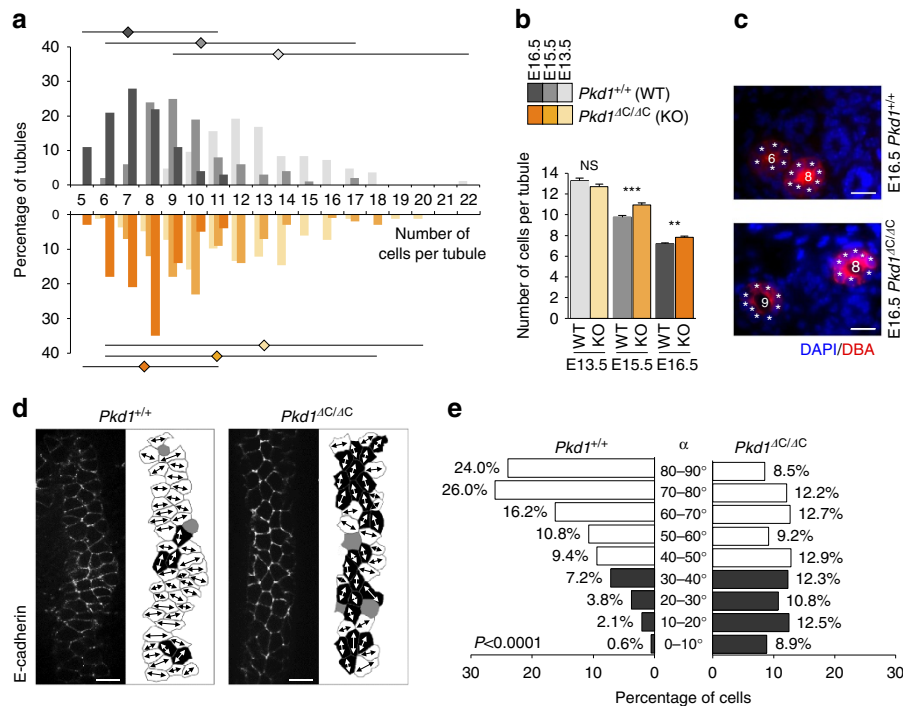


**Figure 1 | Defective tubular narrowing and cellular morphology in *Pkd1* mutants.** (a) Histogram of the percentage (y axis) of DBA-positive tubules with a given number of cells (x axis) per tubule cross-section at E13.5, E15.5 and E16.5 in wt (top, grey bars) or *Pkd1<sup>ΔC/ΔC</sup>* (bottom, orange bars) kidneys. The squares and bars on top show the average and the distribution (maximum and minimum numbers), respectively. (b) Graph extrapolated from the data in a. Histograms and bars represent the average and s.e.m. At E13.5,  $n = 183$  (wt) and  $n = 182$  (KO), and at E15.5 and E16.5,  $n = 200$  for both the genotypes, where  $n$  indicates the number of tubules counted. Statistical analysis was carried out by analysis of variance followed by the Bonferroni parameter. NS, nonsignificant; \*\* $P < 0.01$ ; \*\*\* $P < 0.001$ . (c) Representative sections of DBA-positive (red) developing tubules at E16.5 of *Pkd1<sup>+/+</sup>* or *Pkd1<sup>ΔC/ΔC</sup>* kidneys. Each cell is labelled with an asterisk and the number of cells per cross-section indicated in the lumen. Scale bar, 20  $\mu\text{m}$ . (d) Confocal images (left panels) and cell outlines (right panels) of frontal sections of E15.5 wt (*Pkd1<sup>+/+</sup>*) or *Pkd1* mutant (*Pkd1<sup>ΔC/ΔC</sup>*) kidneys stained with an antibody to E-cadherin in DBA-positive sections. Images in the left panels represent sections two frames basal to the aPKC staining, as previously described<sup>4</sup>. Mediolaterally elongated cells are labelled in white, proximal–distally in black, non-elongated cells in grey. Scale bar, 10  $\mu\text{m}$ . (e) Quantification of the angle of cellular elongation relative to the proximal–distal axis of the tubule for *Pkd1<sup>+/+</sup>* (left) and *Pkd1<sup>ΔC/ΔC</sup>* (right). The percentage of cells within each 10° increment is shown. White bars represent cells elongated mediolaterally within a 40°–90° angle. Cells for wt ( $n = 530$ ) and for mutants ( $n = 575$ ) were counted in a minimum of six kidneys from three litters.  $P < 0.0001$ . Statistical analysis was performed using the Mann–Whitney test.

mediating OCD in the tubules of newborn kidneys has been recently investigated and led to controversial results<sup>8,9</sup>, whereas the role of PC-1 in tubular morphogenesis and CE during development was not investigated.

Here we show that PC-1 is essential for a proper establishment of tubular diameter and mediolateral cell orientation during embryonic renal development in the mouse. PC-1 directly associates with Par3 and favours the association of a Par3/atypical protein kinase C (aPKC) complex in a process likely to be important for oriented cell migration and for renal tubular morphogenesis in the developing kidney. In line with this, we also find that inactivation of the *Par3* gene in the developing kidneys leads to defective CE and to a non-fully penetrant renal cystic phenotype.

**Results**

**Defective CE in *Pkd1<sup>AC/AC</sup>* kidneys.** To test whether PC-1 is involved in CE during renal development, we analysed a *Pkd1* mutant allele previously described by our group, which lacks the last two exons of the gene, resulting in a mutant protein lacking the intracellular C-tail (*Pkd1<sup>AC/AC</sup>*)<sup>10</sup>. These mice die between E16.5 and E17.5, and display renal cyst formation starting at E15.5 similar to other PKD mice models. The number of cells per cross-section of DBA (*Dolichos biflorus* agglutinin)-positive renal tubules in wild-type (wt) kidneys decreased over time from E13.5 to E16.5 (Fig. 1a,b), indicating that their diameter decreases (Supplementary Fig. S1). Analysis of *Pkd1<sup>AC/AC</sup>* mutants showed no significant difference from wt at E13.5 (Fig. 1a,b), but a significant defect in tubular narrowing as compared with the wt

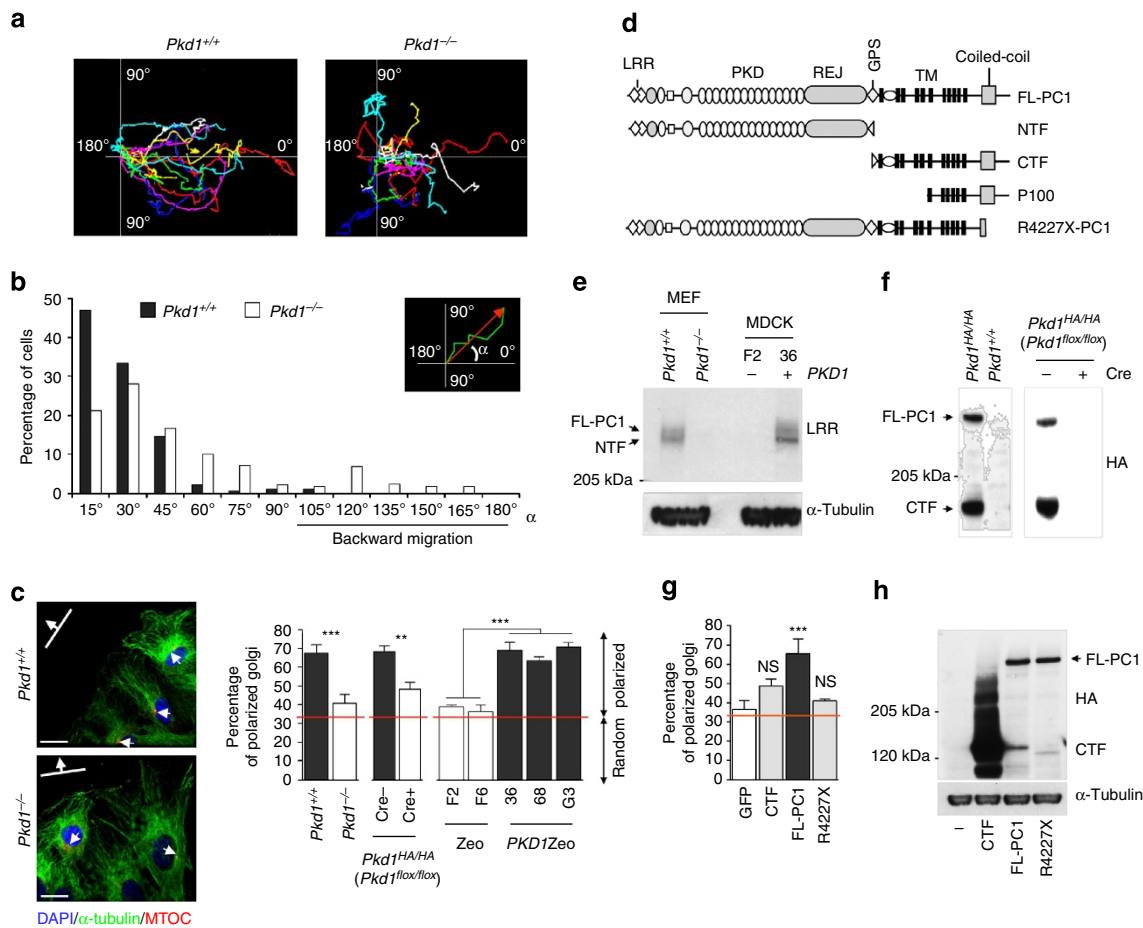


**Figure 2 | PC-1 controls polarized migration.** (a) Tracking of cells of *Pkd1<sup>+/+</sup>* and *Pkd1<sup>-/-</sup>* MEFs in 12-h wound-healing time-lapse experiments. Each coloured line is a cell. (b) Scheme and quantification of the experiments in a. The angle of deviation  $\alpha$  of each trajectory from a theoretical linear migration (equal to angle  $0^\circ$ ) was calculated. Cells ( $n=102$ ) from nine movies in three independent experiments per cell line. Statistical analysis was performed using the Mann-Whitney test.  $P < 0.0001$ . (c) Left, *Pkd1<sup>+/+</sup>* or *Pkd1<sup>-/-</sup>* MEFs subject to wound healing followed by IF with an anti- $\alpha$ -tubulin (green), anti-pericentrin (red) and DAPI (blue). Scale bar, 20  $\mu\text{m}$ . Right, quantification of front-rear polarity on three independent MDCK<sup>PKD1Zeo</sup> clones (36, 68 and G3) and two independent MDCK<sup>Zeo</sup> (F2 and F6), on *Pkd1<sup>+/+</sup>* or *Pkd1<sup>-/-</sup>* MEFs or *Pkd1<sup>fllox/fllox</sup>* MEFs treated or not with a Cre-recombinase. The red line shows a theoretical random distribution (33%). Statistical analysis was performed using the Student's *t*-test (for MEFs, left) or analysis of variance (ANOVA; for PKD clones, right) followed by the Bonferroni parameter.  $**P < 0.01$ ;  $***P < 0.001$ . Data are means  $\pm$  s.d. and are representative of a minimum of three independent experiments performed in triplicate, in which at least 300 cells were counted. (d) Diagram of PC-1 different isoforms and/or mutant constructs. (e) Immunoblotting of PC-1 in fibroblasts or in MDCK<sup>PKD1Zeo</sup> (36) and MDCK<sup>Zeo</sup> (F2) using an anti-LRR antibody (7e12, see Methods), detects both the full-length (FL-PC-1, ~520 kDa) and the cleaved, N-terminal fragment (NTF, ~400 kDa). No signal is observed in *Pkd1<sup>-/-</sup>* cells. (f) Immunoblotting of endogenous tagged PC-1 using an anti-HA detects two bands corresponding to the full-length uncleaved PC-1 (FL-PC-1, ~520 kDa) and the C-terminal fragment (CTF, ~150 kDa). Treatment with a Cre-recombinase causes disappearance of FL-PC-1-HA detection. (g) MDCK type-II cells were transiently transfected with green fluorescent protein alone or along with full-length PC-1 (FL-PC-1), the R4227X or the CTF HA-tagged mutants. After sorting, cells were treated as in c. Data are means  $\pm$  s.d.; Statistical analysis was performed using ANOVA followed by Bonferroni parameter.  $***P < 0.001$ , NS, nonsignificant.

tubules at later stages (E15.5 and E16.5, Fig. 1a,b,c and Supplementary Fig. S1). Staining with Ki67, terminal transferase dUTP nick-end labelling (TUNEL) and cleaved caspase-3 revealed that neither differences in proliferation nor in apoptosis could account for the differences between *Pkd1*<sup>+/+</sup> and *Pkd1*<sup>ΔC/ΔC</sup> tubules (Supplementary Fig. S1). Conversely, analysis of the morphology of epithelial cells in DBA-positive tubules revealed that the mediolateral orientation normally observed in wt was lost in *Pkd1*<sup>ΔC/ΔC</sup> developing kidneys at E15.5 (Fig. 1d,e and Supplementary Fig. S1).

### PC-1 regulates the front–rear polarity and oriented migration.

We next aimed at investigating the molecular mechanism underlying this defect. Unfortunately, an appropriate functional assay to study CE or planar polarity *in vitro* is not available. However, the process of CE is intimately linked to the capability of cells to migrate and orient correctly. Therefore, we used cells derived from *Pkd1*<sup>+/+</sup> or *Pkd1*<sup>-/-</sup> mice (mouse embryonic fibroblasts, MEFs), in which we have previously reported a defect in migration rates<sup>11</sup>. During our assays, we noticed that in

wound-healing assays *Pkd1*<sup>-/-</sup> MEFs took a contorted path to fill the wound, whereas wt cells migrated in a more linear manner (Fig. 2a,b). Furthermore, *Pkd1*<sup>-/-</sup> cells failed to relocate their microtubule organizing centre and Golgi in front of their nuclei to generate front–rear polarity as observed in wt cells<sup>12,13</sup> (Fig. 2c).

Next, we isolated MEFs derived from a mouse model expressing a floxable haemagglutinin (HA)-tagged endogenous PC-1 (*Pkd1*<sup>HA/HA</sup> or *Pkd1*<sup>flox/flox</sup> interchangeably)<sup>10</sup>. As previously described, HA tags were inserted in-frame into the last exon of the *Pkd1* gene, resulting in the expression of HA-tagged endogenous PC-1 (ref. 10, Fig. 2f). These lines also carry loxP sites flanking exon 45 and exon 46 (ref. 10). Therefore, on treatment with a Cre-recombinase, *Pkd1*<sup>HA/HA</sup> generate the *Pkd1*<sup>ΔC/ΔC</sup> alleles described above, which have lost the protein's C terminus and its detectability (Fig. 2c,f). Importantly, we found that these cells have lost their capability to polarize in wound-healing assays (Fig. 2c).

Furthermore, a set of Madin–Darby canine kidney, type-II (MDCK type-II) cells overexpressing PC-1 (ref. 14) acquired a polarized migratory phenotype as compared with controls (Fig. 2c). Finally, transient overexpression of wt FL-PC-1, but

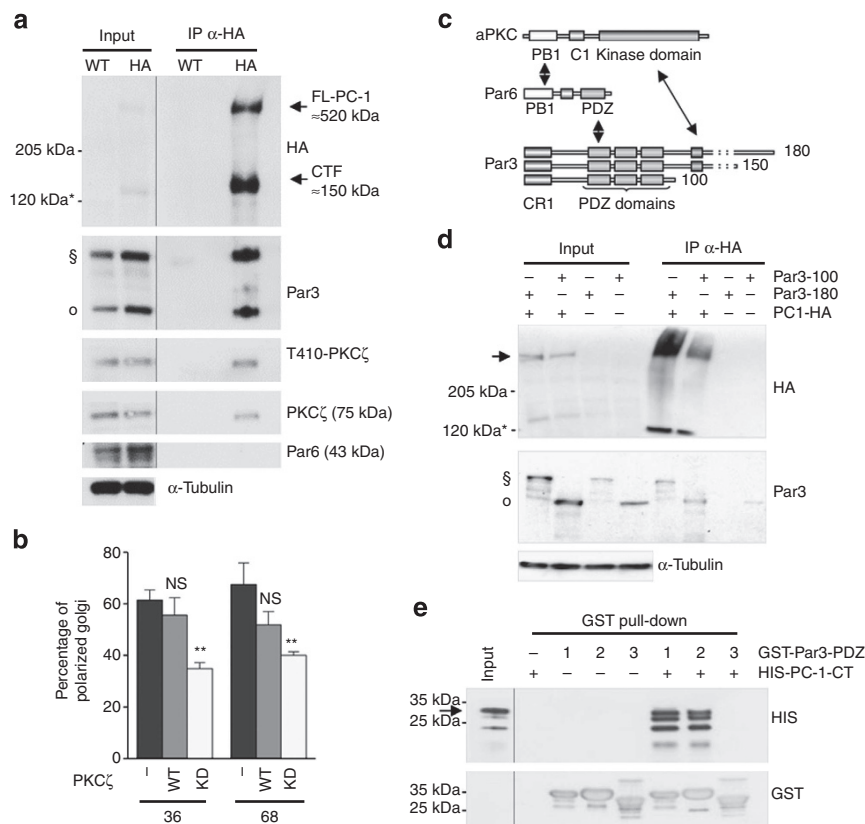


**Figure 3 | PC-1 interacts with the Par3/aPKC complex.** (a) MEFs isolated from a mouse model carrying HA-tagged endogenous PC-1 (ref. 10) or from littermate embryos (wt) were subject to IP with anti-HA antibodies. Western blotting using anti-HA antibodies revealed the presence of both full-length (arrow, ~520 kDa) as well as cleaved C-terminal fragment (CTF; \*, ~150 kDa) isoforms of endogenous, tagged PC-1. Immunoblot analysis of the same IPs using anti-PKCζ and anti-phosphoThr410-PKCζ revealed that PKCζ (78 kDa) interacts with PC-1 in its active form; analysis using anti-Par3 antibodies reveals that PC-1 also coprecipitated with Par3 (180 kDa (§)) and Par3 (100 kDa (°)); analysis using anti-Par6 (43 kDa) antibodies revealed that this molecule is not immunoprecipitated. Blot is representative of multiple independent experiments. (b) Transient transfection of a kinase-dead mutant (KD-PKCζ) or a wt form (WT-PKCζ) in two MDCK<sup>PKD1Zeo</sup> clones (68 and 36). Data are means ± s.d. Statistical analysis was performed using analysis of variance followed by Bonferroni parameter. \*\**P* < 0.01. NS, nonsignificant. (c) Schematic representation of the aPKC, Par6 and three different isoforms of Par3; arrows indicate the described interacting domains. (d) Hek293T cells were transiently transfected with HA-tagged full-length PC-1 (PC-1-HA) along with the 180 and 100 kDa forms of YFP-Par3, followed by IP with anti-HA antibodies. The blot is representative of two independent experiments. (e) GST-tagged versions of each of the three PDZ domains of Par3 were immobilized on G-sepharose beads, and subsequently incubated with HIS-PC-1-CT. Immunoblotting with anti-GST revealed that equal amounts of GST-PDZ domains of Par3 were immobilized on the beads. Anti-HIS showed that PC-1-CT interacts with the first two PDZ domains, but not with the third.



not of the patient-derived mutant R4227X (ref. 15) or the C-terminal fragment<sup>16</sup>, induced front–rear polarity (Fig. 2g,h). Thus, in addition to the previously described capability of PC-1 to regulate cell motility<sup>11</sup>, here we show that PC-1 also regulates the front–rear cell polarity during migration and both the C- and the N-terminal domains are required for this activity.

**PC-1 binds the Par3/aPKC complex.** Although the capability of cells to reach appropriate front–rear polarity cannot be considered as an *in-vitro* assay for CE, the two processes share some molecular factors and mechanisms. One of these is the complex composed of aPKC and the polarity proteins Par3 and Par6, which is very important both for front–rear polarity in mammalian cells and for CE in flies and lower vertebrates<sup>13,17–20</sup>. Therefore, we investigated whether PC-1 could interact or regulate components of the Pars/aPKC complex. To this end,

we used MEFs isolated from *Pkd1*<sup>HA/HA</sup> knock-in mice (Fig. 2f)<sup>10</sup>. Immunoprecipitation (IP) studies revealed that PC-1 coprecipitates with aPKC, a fraction of which reveal phosphorylation in Thr410 (Fig. 3a). In line with this, a kinase-dead mutant of aPKC abrogates the front–rear polarity in MDCK<sup>PKD1Zeo</sup> cells, suggesting that this kinase is important (Fig. 3b), and, in line with published studies, the same mutant abrogated the front–rear polarity in wt MEFs (Supplementary Fig. S2). Notably, endogenous PC-1 coprecipitated Par3 but not Par6 in *Pkd1*<sup>HA/HA</sup> MEFs (Fig. 3a), and in reverse IP studies Par3 coprecipitated PC-1 in *Pkd1*<sup>HA/HA</sup> MEFs (Supplementary Fig. S2). To define the domains involved in the interaction, we overexpressed the full-length HA-tagged PC-1 with the 180 kDa or the 100 kDa form of Par3, lacking the aPKC-binding domain (Fig. 3c), and found that the overexpressed PC-1 coprecipitated both isoforms (Fig. 3d). Furthermore, when the same two constructs were transfected into *Pkd1*<sup>HA/HA</sup> MEF lines, we found that

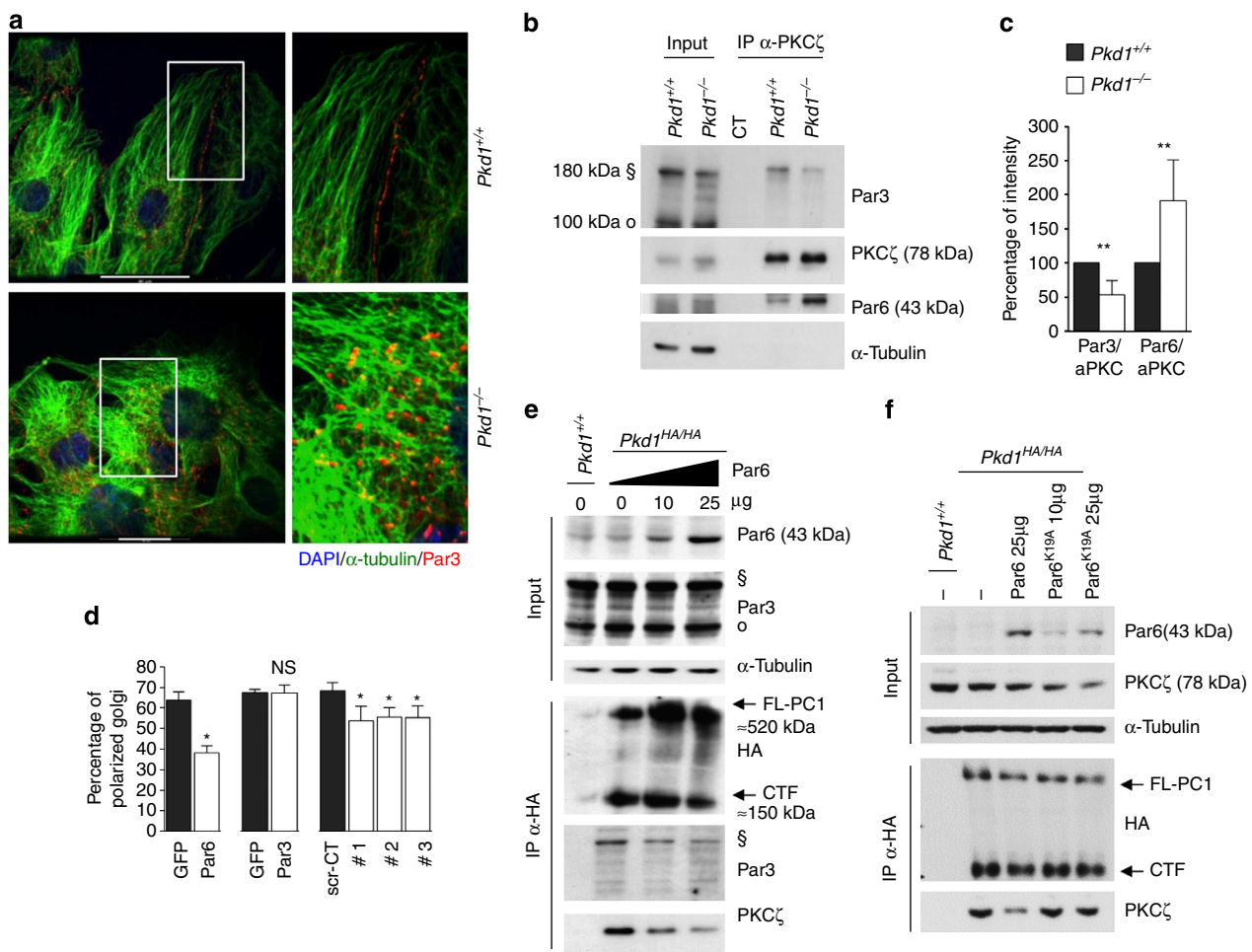


**Figure 4 | PC-1 can influence the ratio of Par3 versus Par6 bound to aPKC.** (a) MEF cells were subject to wound, fixed and stained for anti-tubulin (green) and anti-Par3 (red). Scale bars, 20 μm. (b) IP from *Pkd1*<sup>+/+</sup> or *Pkd1*<sup>-/-</sup> MEFs using an anti-PKCζ antibody followed by immunoblotting with an anti-Par3 (180, 150 and 110 kDa) or anti-Par6 (43 kDa) antibody, in *Pkd1*<sup>+/+</sup> and *Pkd1*<sup>-/-</sup> MEFs. CT, cell lysate from *Pkd1*<sup>+/+</sup> MEFs was incubated in the absence of primary anti-PKC antibody. The blot is representative of seven independent experiments. (c) Quantification of the intensity of bands from seven independent experiments carried out as in b. Data are means ± s.e.m. Statistical analysis was performed using analysis of variance (ANOVA) followed by Bonferroni parameter. \*\**P* < 0.01. (d) Green fluorescent protein (GFP)-positive cells, transfected with GFP, Par6 (GFP, bicistronic vector) or Par3 (180 kDa, YFP-tagged, *n* = 50–120), as well as transfected with three Par3 short interfering RNA (number #1–3, *n* = 600), were analysed for the capability to polarize in wound-healing assays as in Fig. 2c. Data are means ± s.d., and representative of three independent experiments performed in triplicate. Statistical analysis was performed using ANOVA followed by Bonferroni parameter. \**P* < 0.05, NS, non-statistically significant. (e) *Pkd1*<sup>+/+</sup> or *Pkd1*<sup>HA/HA</sup> MEFs were transfected with increasing amounts of Par6A-expressing constructs, followed by IP with anti-HA beads, followed by western blot analysis with anti-aPKC (78 kDa), anti-Par3 (180 kDa), anti-Par6 (43 kDa) or anti-HA antibodies (full-length PC-1 ~ 520 kDa and C-terminal fragment (CTF) ~ 150 kDa). (f) The experiment was performed as in e, except that the *Pkd1*<sup>HA/HA</sup> MEFs were transfected with Par6 or Par6<sup>K19A</sup> construct (43 kDa), mutated in the aPKC-binding site<sup>22</sup>.

endogenous PC-1 can also interact with both isoforms (Supplementary Fig. S2). Next, we expressed in bacteria the three PDZ domains of Par3, each fused to glutathione S-transferase (GST), and used them in GST pull-down assays along with a histidine-tagged intracellular C-terminal tail of PC-1 (HIS-PC-1-CT)<sup>21</sup>. We found that HIS-PC-1-CT binds to the first two PDZ domains of Par3, but not to the third one (Fig. 3e). We conclude that PC-1 C-tail associates directly with Par3 through its first two PDZ domains. These results along with the capability of PC-1 to interact with Par3 lacking the aPKC-binding domain suggest that probably Par3 mediates the interaction between PC-1 and aPKC.

### PC-1 regulates a balance between Par3/aPKC and Par6/aPKC.

Next, we looked at the distribution of Par3 in *Pkd1*<sup>-/-</sup> MEFs subject to wound healing and found that these cells fail to properly localize Par3 in distinct patches aligned along the cell-cell contacts, as in wt cells and as previously reported<sup>13</sup> (Fig. 4a). Furthermore, IP of aPKC from *Pkd1*<sup>+/+</sup> and *Pkd1*<sup>-/-</sup> cells revealed that its association with Par3 is reduced, whereas its association with Par6 is enhanced (Fig. 4b,c). We hypothesized that changes in the ratio of the Par3 or Par6 bound to aPKC might influence polarized migration. Indeed, overexpression of Par6A was able to displace Par3 from aPKC (Supplementary Fig. S3) and caused an impairment of the front-rear polarity (Fig. 4d). Overexpression of Par3 did not have an effect on

polarity (Fig. 4d), whereas its silencing impaired the front-rear polarity (Fig. 4d and Supplementary Fig. S3). Importantly, overexpression of wt Par6A in *Pkd1*<sup>HA/HA</sup> fibroblasts competes away the association between PC-1 and aPKC in a dose-dependent manner (Fig. 4e). Using a Par6 mutant (Par6<sup>K19A</sup>), which lacks the capability to bind aPKC<sup>22</sup>, we found that the interaction between Par6 and aPKC is required for its competing activity (Fig. 4f), suggesting that Par6 subtracts aPKC from PC-1/Par3 by binding directly to aPKC. Thus, PC-1 associates with a Par3/aPKC complex (which is in competition with a Par6/aPKC complex) to regulate the front-rear polarity.

**PC-1 and Par3 associate *in vivo*.** As the Par3/aPKC complex was reported to regulate CE in *Drosophila* and lower vertebrates<sup>20,23,24</sup>, we next investigated whether PC-1 interaction with Par3/aPKC could be detected *in vivo* using our unique murine model of tagged endogenous PC-1 (ref. 10). First, we found that the expression levels and cleavage products of PC-1 in the developing kidney in the time window when CE occurs (E13.5 to P1, Fig. 5a–c) are regulated. Notably, the full-length uncleaved PC-1 levels are maximal in the kidney at E13.5 and progressively decrease during development up to birth; although it is visible in longer exposure times (Fig. 5c), the cleaved C-terminal fragment increases progressively and the P100 (ref. 25) only appears in the newborn kidneys (Fig. 5c). Importantly, the expression pattern of

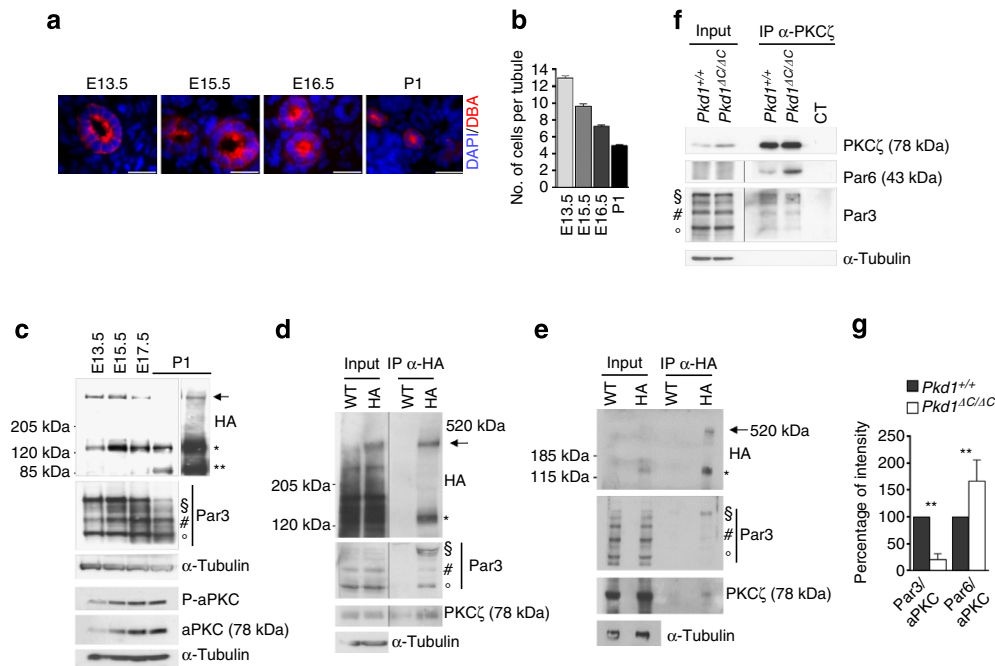


**Figure 5 | PC-1 interacts with and regulates Par3/aPKC in the developing kidneys.** (a) Images of DBA-positive tubules at the stages indicated show narrowing of the tubules. Scale bar, 20  $\mu$ m. (b) Histogram quantifying the process illustrated in a; graphs are average  $\pm$  s.e.m. of the number of cells per tubule cross-section. (c) Western blot analysis on lysates derived from pools of E13.5, E15.5, E17.5 and P1 developing kidneys from *Pkd1*<sup>HA/HA</sup> mice, using anti-HA (top panel), anti-Par3 (middle panel) and anti-phosphorylated (T410), or total levels of aPKC antibodies (bottom panel). Representative western blotting of three independent experiments. Arrow, full-length PC-1 (~520 kDa); \*, C-terminal fragment (CTF) cleavage product of PC-1 (~150 kDa); \*\*, P100 cleavage product of PC-1 (~100 kDa); §, 180 kDa Par; #, 150 kDa Par3; °, 100 kDa Par3. (d) E15.5 total embryo lysates from *Pkd1*<sup>HA/HA</sup> (HA) or *Pkd1*<sup>+/+</sup> (wt) mice were used to immunoprecipitate PC-1 using anti-HA antibodies, followed by immunoblotting with anti-HA (top), anti-Par3 (middle) or anti-PKC $\zeta$  antibodies (bottom). Arrow, full-length PC-1 (~520 kDa); \*, CTF cleavage product of PC-1 (~150 kDa); §, 180 kDa Par; #, 150 kDa Par3; °, 100 kDa Par3. (e) PC-1 was immunoprecipitated from kidneys of *Pkd1*<sup>HA/HA</sup> or *Pkd1*<sup>+/+</sup> at E17.5 using anti-HA antibodies, followed by immunoblotting with anti-HA, anti-Par3 and anti-aPKC antibodies. Arrow, full-length PC-1 (~520 kDa); \*, CTF cleavage product of PC-1 (~150 kDa); §, 180 kDa Par. (f) IP analysis from E16.5 *Pkd1*<sup>+/+</sup> or *Pkd1*<sup>ΔC/ΔC</sup> kidneys using an anti-PKC $\zeta$  antibody followed by immunoblotting with an anti-Par3 or anti-Par6 (43 kDa) antibody. CT, cell lysate from *Pkd1*<sup>+/+</sup> embryonic kidneys was incubated in the absence of primary anti-PKC antibody. The blot is representative of three independent experiments. (g) Quantification as means  $\pm$  s.e.m. of the intensity of bands from three independent experiments performed as in f. Statistical analysis was performed using analysis of variance followed by Bonferroni parameter. \*\* $P < 0.01$ .

Par3, and specifically the 180 kDa isoform<sup>26</sup>, overlaps with that of full-length PC-1. Second, IP of endogenous HA-PC-1 resulted in coprecipitation of Par3 and aPKC in total embryos at E15.5 (Fig. 5d), in the developing kidneys at E17.5 (Fig. 5e and Supplementary Fig. S2) and in P1 newborn kidneys (Supplementary Fig. S2). Finally, we analysed the aPKC complexes and found that IP of aPKC reveals that it preferentially associates with Par3 in *Pkd1*<sup>+/+</sup> E17.5 kidneys, whereas it preferentially associates with Par6 in E17.5 *Pkd1*<sup>ΔC/ΔC</sup> mutant kidneys (Fig. 5f,g). These data are in line with the composition of the complexes observed in cells (Fig. 4b,c). As the *Pkd1*<sup>ΔC/ΔC</sup> mutants lack the intracellular C-tail of PC-1, our studies support the notion that this region is essential for PC-1 proper function during renal tubular morphogenesis.

**Defective CE in Par3-mutant kidneys.** We next reasoned that if direct interaction between PC-1 and Par3 is essential to mediate correct CE and renal tubular narrowing, we would predict that mice mutant for *Par3* display a similar defect than *Pkd1* mutants. Homozygous deletion of *Par3* results in embryonic lethality before

E12.5, preventing the analysis of renal development<sup>27</sup>. Thus, we intercrossed a line harbouring a conditional allele for *Par3* (ref. 27) with a line carrying a *Hoxb7:Cre* (confining Cre expression in the UB)<sup>28</sup>. Staining of anti-Par3 antibodies confirmed that the protein is lost in a high percentage of cells at E15.5 and at P1 (Supplementary Fig. S4). The resulting mice (*Hoxb7Cre; Par3*<sup>lox/-</sup>) displayed a defective number of cells per tubular cross-sections in DBA-positive tubules at E16.5 (Fig. 6a,b). Importantly, the *Par3* mutants displayed a defective mediolateral orientation of epithelial cells (Fig. 6c). A defective number of cells per tubular cross-sections was also observed at P1 (Fig. 6a,b), when a few cysts and tubular dilatations were also observed in four out of ten *Hoxb7Cre; Par3*<sup>lox/-</sup> mice (Fig. 6d). Importantly, in E15.5 DBA-positive tubules, the rates of cell division were not affected in the *Par3* mutants, whereas apoptosis was slightly increased (Supplementary Fig. S4). Furthermore, analysis of markers of apico-basal polarity and tight junctions formation revealed no major defects at this level in the epithelia lacking *Par3* (Fig. 6e and Supplementary Fig. S4), in line with previously published studies<sup>26</sup>. We conclude that indeed *Par3* is essential for proper CE during renal development in the mouse and that this

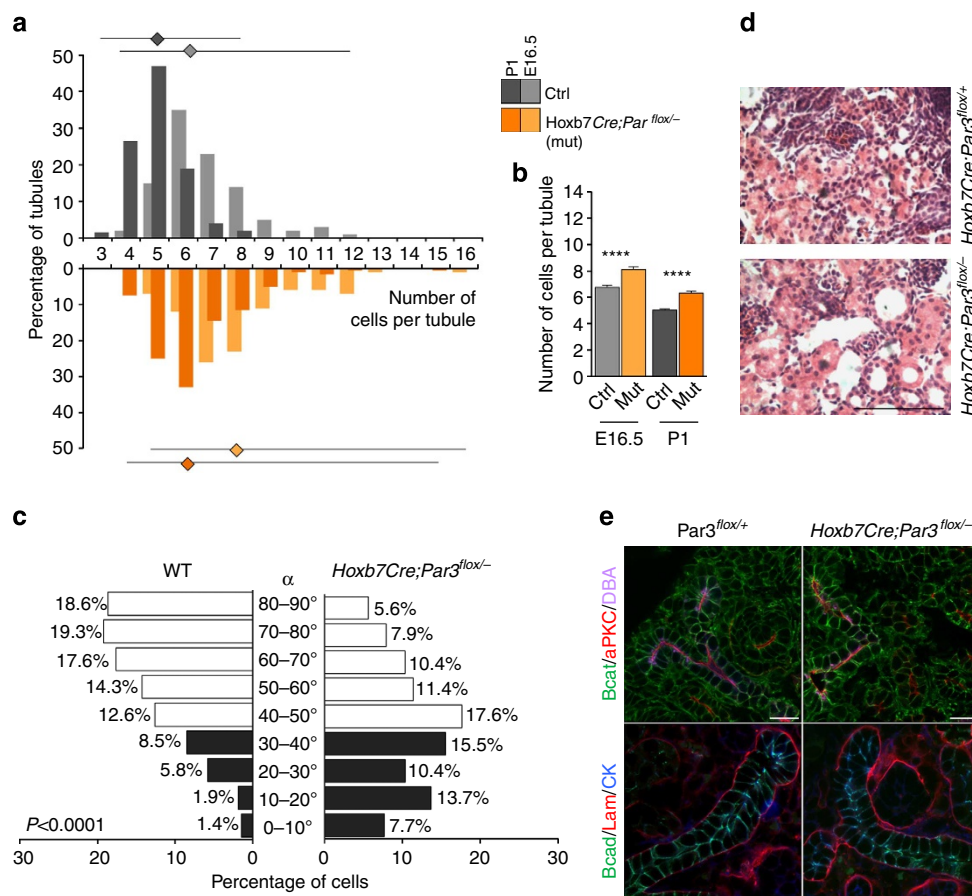


**Figure 6 | Defective CE in Par3 mutants.** (a) Histograms showing the distribution of the number of cells per cross-section of tubules as in wt (grey bars,  $n = 100$ ) and *Hoxb7Cre;Par3*<sup>lox/-</sup> mutant (orange bars,  $n = 100$ ) developing kidneys at E16.5 or P1;  $n$  indicates the number of tubules counted. CTRL, controls are either *Hoxb7Cre;Par3*<sup>lox/+</sup> (at P1) or *Par3*<sup>lox/-</sup> (at E16.5). (b) Graph extrapolated from the data in a; histograms and bars represent the average and s.e.m. Statistical analysis was performed by analysis of variance (ANOVA) followed by Bonferroni parameter. \*\*\*\* $P < 0.0001$ . (c) Quantification of the angle of cellular elongation relative to the proximal-distal axis of the E15.5 tubule for wt or *Hoxb7Cre;Par3*<sup>lox/-</sup> (right), as in Fig. 1e. Four hundred and eighty-three cells for wt and mutants in a minimum of six kidneys from three litters were counted.  $P < 0.0001$ . Statistical analysis was performed using the Mann-Whitney test. (d) Haematoxylin and eosin staining of *Hoxb7Cre;Par3*<sup>lox/+</sup> and *Hoxb7Cre;Par3*<sup>lox/-</sup> mutant kidneys at P1 show tubular dilatation and small cysts in the *Par3* mutants. Scale bar, 100  $\mu\text{m}$ . (e) Sections of control (*Par3*<sup>lox/+</sup>, left panel) and mutant (*Hoxb7Cre;Par3*<sup>lox/-</sup>, right panel) P1 kidneys stained with antibodies to aPKC (red),  $\beta$ -catenin (green) and the collecting duct maker DBA (purple) in the top panel. In the bottom panel, sections were stained with Laminin (red), E-cadherin (green) and the collecting duct marker cytokeratin (blue). No differences were observed in protein localization/polarity between control and mutant collecting ducts. Scale bar, 20  $\mu\text{m}$ .



process is independent of Par3 function in apico-basal polarity, but possibly relies on PCP, as recently demonstrated<sup>5</sup>.

## Discussion

In this study, we have uncovered a critical role for PC-1 in the recently described CE process essential to achieve proper tubular elongation and morphogenesis. In wt developing kidneys, DBA-positive tubules are composed of an average of 13 cells at E13.5 and an average of 7 cells by E16.5. We have shown that in *Pkd1* mutant kidneys, DBA-positive tubules fail to undergo this programme of tubular narrowing. Previous studies have shown that the epithelium of the developing nephron divides in a non-oriented manner, but it undergoes mediolateral cellular orientation<sup>4</sup>. As this is a hallmark of tissues undergoing a programme of CE to achieve elongation and narrowing<sup>29,30</sup>, this prompted investigators to hypothesize and, subsequently, to demonstrate that the developing nephron is shaped through CE-like movements<sup>3,4</sup>. Indeed, cellular intercalation appears to be the mechanism that best explains how epithelial tubules can narrow over time. Here we have shown that the epithelium of DBA-positive tubules lacking functional PC-1 fails to orient mediolaterally, suggesting that PC-1 has an essential role in this process. Our study further uncovers a role for PC-1 in regulation of a programme of cell polarity, enabling cells to properly achieve cellular elongation and front-rear asymmetry during migration in wound-healing assays. We have shown that PC-1 interacts with the aPKC/Par3 (180 kDa) complex and probably regulates it to achieve polarized cell migration.

It is interesting to note that PC-1 interacts with both Par3 and aPKC, but not with Par6. Furthermore, the biochemical composition of the aPKC-containing complexes appears to be altered in *Pkd1* mutant cells and kidneys. In wt cells, which are able to properly polarize during migration, aPKC preferentially binds to Par3. In contrast, in cells lacking functional PC-1 aPKC appears to preferentially bind to Par6. In addition, overexpression of Par6 is able to compete with Par3 for binding to aPKC and, in line with this, it is able to subtract aPKC from the PC-1/Par3/aPKC complex. This prompted us to hypothesize that Par6 and Par3 might actually compete for binding aPKC. Our data are in line with previous models proposed mostly based on studies in *Drosophila*, demonstrating that Bazooka (Par3) and Par6 can associate into distinct complexes with different functional roles<sup>31</sup>. Furthermore, a recent study has demonstrated that a competitive binding between Crumbs and Par6 can modulate the exclusion of Par3 from the Par6/aPKC complex, providing further support for a fine-tuned regulation of the so-called 'Par6/Par3/aPKC complex' by competitive binding<sup>31</sup>.

It is noteworthy that Par3 (180 kDa isoform) and PC-1 appear to follow a similar developmental regulation that parallels the timing of tubular morphogenesis described above. The two proteins are associated *in vivo* in total embryos and in the developing kidney. We hypothesized that this association might be essential for regulating mediolateral cell orientation and CE during renal tubular morphogenesis. The essential role of the Pars/aPKC complex in regulation of CE downstream of the PCP has been demonstrated in *Drosophila melanogaster*<sup>20,24</sup>, whereas a single study has implicated their role in lower vertebrates<sup>19</sup>. Here we have demonstrated that inactivation of *Par3* in the UB of the developing kidney results in defective narrowing of the tubular diameter and defective mediolateral orientation of the epithelia composing these tubules. Thus, our data imply, for the first time, a role of Par3 in CE and tubular morphogenesis in a mammalian system.

Although our studies provide important novel insight in the function of PC-1 and its role in renal development, one important

question that remains unanswered is whether and how defective CE might result in cyst formation. We show that only ~40% of the *Hoxb7Cre:Par3<sup>fllox</sup>/-* mice develop cysts. Thus, defective CE alone might not be sufficient to cause cyst formation and compensatory mechanisms might exist. Similarly, in a previous study, Nishio *et al.*<sup>8</sup> have shown that defective OCD does not initiate cyst formation in the newborn kidney, as mice mutant for *Pkhd1* display defective OCD but not cyst formation. It was proposed that a compensatory mechanism of intercalation might prevent cyst formation in these mice. Thus, one possibility is that neither defects in OCD nor in CE alone are sufficient to initiate cyst formation, but they both might contribute.

In summary, in this study we have described a novel role for PC-1 in regulation of a programme of cell polarity, which is important to achieve proper tubular morphogenesis during renal development. Further studies will be required to assess whether this biological function of PC-1 is important for preventing cyst formation and it is relevant for the disease.

## Methods

**Antibodies and inhibitors.** Anti- $\alpha$ -tubulin and anti-flag antibodies were obtained from Sigma (catalogue number 77418-1EA, T5168, T6793 and F1804). Anti phospho-PKC $\lambda/\zeta$  (Thr410/403; catalogue number 9378) was obtained from Cell Signaling. DAPI (catalogue number sc-3598), anti-PKC $\zeta$  (sc-216/sc-216-G), anti-Par6 (catalogue number sc-14405), anti-PC-1 (catalogue number sc-130554), anti-His (catalogue number sc-8036) and anti-GST (catalogue number sc-495) were obtained from Santa Cruz. Anti-HA from Roche (rat monoclonal catalogue number 13948000). Anti-Par3 was obtained from Millipore (catalogue number 07-330, diluted at 1:300 for immunofluorescence (IF) and at 1:1,000 for western blot). Anti-E-cadherin was obtained from Invitrogen (catalogue number 131900). Anti-Giantin (catalogue number PRB-114C) and anti-pericentrin (catalogue number PRB-432C) were obtained from Covance. Anti-ezrin was obtained from Millipore (07-130, 1:100); anti-occludin from Invitrogen (71-1500, 1:500); and anti-beta-catenin (C7207, 1:500), anti-laminin (I9393, 1:500) and anti-CK from Sigma (C2562, 1:500). Rhodamine conjugated-DBA was obtained from Vector Laboratories (cat RL-1032). All primary antibodies were diluted according to the manufacturer's instructions unless otherwise stated. HRP-conjugated secondary antibodies (GE Healthcare) were diluted at a 1:7,000 and detection was made with an ECL system (Amersham).

**Analysis of *Pkd1* mutant mice.** The *Pkd1<sup>AC</sup>* mouse model has been previously generated and carries loxP sites flanking the last two exons of the *Pkd1* gene (exons 45 and 46)<sup>10</sup>. Timed pregnant mice were obtained by overnight crossing wt or *Pkd1<sup>AC/+</sup>* mice in 100% Bl6/57, and checking for vaginal plugs the next morning. The presence of a vaginal plug was defined as gestational day E0.5 (embryonic day 0.5). All embryos were collected at the defined embryonic stages (between E13.5 and P1 as specified in the legends) and were 50% females and 50% males. The wt and mutant live (based on heart beating) littermate embryos were evaluated from a minimum of three independent litters. All animal care and experimental protocols on the *Pkd1* mutants were conducted upon approval of a specific protocol (IACUC-548) by the Institutional Care and Use Ethical Committee at the San Raffaele Scientific Institute. For biochemical studies, we collected and pooled kidneys at day E13.5, 15.5, E17.5 or P1, lysed them with 0.5% triton lysis buffer; IPs were performed as described below for *in-vitro* studies.

**Evaluation of tubular diameter *in vivo*.** For the evaluation of the number of cells/tubular cross-section, 12  $\mu$ m sections of E13.5, 15.5, 16.5 or P1 kidneys were stained with the DBA marker and the nuclear marker DAPI. Nuclei of circle-shaped kidney DBA-positive tubules were counted, excluding from analysis the oval-shaped tubules that have values of ovality at the ImageJ software <0.995 (that is, tubules that are not perpendicularly cross-sectioned). We performed two independent experiments for E13.5, E15.5 and E16.5 live (based on heart beating) littermate embryos, counting 100 wt and 100 mutant tubules for each experiment, as well as for P1 wt kidneys. Whenever the phenotype of the embryos was not overt, the analyses were performed in a blinded manner. For the evaluation of circumference and diameter, for round-shaped tubules, a circumference was tracked going through the centre of all the nuclei of the tubular section; the measure of the circumference and of the related Feret's diameter was quantified by ImageJ software.

**Evaluation of cellular orientation *in vivo*.** For the evaluation of cell elongation and orientation, E15.5 embryos were fixed on in ice-cold methanol, included in 5% low-melting agarose, cut in 100- to 150- $\mu$ m sections with a vibratome and stained with DBA, anti-E-cadherin, anti-PKC $\zeta$  antibodies and DAPI. Z-stacks of renal



tubules were captured every 1  $\mu\text{m}$ , using UltraView spinning disk confocal microscope (PerkinElmer) with Velocity software. For the evaluation of medio-lateral orientation, cell shape was tracked using the automated Magnetic Lasso tool (Photoshop), on E-cadherin staining in sections taken two frames below (basal to) PKC staining. Only cells in the image where E-cadherin staining outlined the entire cell were used for calculations (cells on the edges that had discontinuous E-cadherin staining were not measured). For all other cells, the length (longest axis) to width (shortest axis) ratio were calculated. Only cells for which the ratio was  $> 1.2$  were considered elongated. Those that have a lower ratio (between 1 and 1.2) are depicted in grey and are not considered elongated. For all the others, the angle between the longest axis of the cell and the longitudinal axis of the tubule were calculated using ImageJ software<sup>4</sup>.

**Apoptosis and proliferation in vivo.** To monitor apoptosis, cryostat kidney sections of 12  $\mu\text{m}$  were stained with TUNEL and the process was carried out using the DeadEnd Fluorometric TUNEL System Kit (Promega), according to the manufacturer's protocol. Sections were costained for DBA and were used at a dilution of 1/100 (Vector Laboratories). For proliferation, sections were permeabilized in TritonX-100 blocked with PBS-BSA 3% and normal goat serum 10% at room temperature for 1 h, incubated overnight with the antibody anti-Ki67 or anti-Phh3 at 4 °C, washed and incubated with secondary antibodies (Alexa Fluor-conjugated secondary antibodies from Invitrogen-Molecular Probes), and DBA was used at a dilution of 1/100. The ProLong Antifade kit (Invitrogen-Molecular Probes) was used for mounting the samples.

**Wound-healing assays.** MDCK type-II and MEF cells were grown on coverslips as high-density monolayers, wounded using a 200- $\mu\text{l}$  pipette tip and allowed to migrate for 3 h (unless otherwise indicated).

For IF studies, paraformaldehyde or methanol-fixed cells were washed, permeabilized in PBS/0.5% Triton X-100 and blocked (PBS, 3% BSA). Primary antibody was applied (all antibodies were diluted to 1:100 in blocking and incubated for 1 h at 37 °C) followed by washes and incubation with secondary antibodies (Alexa Fluor-conjugated secondary antibodies from Invitrogen-Molecular Probes). The ProLong Antifade kit (Invitrogen-Molecular Probes) was used for mounting the samples. Digital images of representative fields were captured using a Zeiss Axiophot fluorescence microscope or UltraView spinning disk confocal microscope (PerkinElmer) equipped with a Plan Apochromat 63X/1.4 oil-immersion objective and using the UltraView ERS acquisition software.

For time-lapse studies, cells on the wound edge were tracked using the public domain ImageJ programme (developed at the National Institutes of Health and available at <http://rsb.info.nih.gov/ij/>). The rate of unidirectional movement was determined following a minimum of ten different cell trajectories from nine movies of three independent experiments (for a total of 102 cells) and measuring the angle formed by the cell trajectories and the perpendicular movement to the wound edge.

**Transfection and cell sorting.** MDCK cells were transiently transfected using Lipofectamine 2000 (Invitrogen). For IP studies, cells were collected at 4 °C in lysis buffer, composed of 150 mM NaCl, 20 mM NaP, 10% glycerol (pH 7.2) supplemented with phosphatase inhibitors (200 mM glycerol phosphate, 200 mM Na orthovanadate and 500 mM Na fluoride), protease inhibitor cocktail (Complete, Roche) and Triton X-100 as indicated, and lysed for 30 min on ice. Nuclei were discarded after centrifugation at 13,200 r.p.m. for 10 min. For HA-tagged PC-1 IP, equal amounts of proteins were incubated overnight at 4 °C with Anti-HA Affinity Matrix (catalogue number 11815016001, Roche); after washes, immunoprecipitates were run on NuPAGE Novex 3–8% TrisAcetate Gel (catalogue number EA0375BOX, Invitrogen). For PKC $\zeta$  IP studies, equal amount of proteins were incubated in rocking with the primary anti-PKC $\zeta$  antibody overnight at 4 °C, then G-sepharose beads (catalogue number 17-0618-01, GE Healthcare) were added and incubated 2 h at room temperature. IPs were followed by immunoblotting with the indicated primary antibodies (see above). For cell-sorting experiments, parental MDCK type-II cells were transiently transfected using Lipofectamine 2000 (Invitrogen) according to the manufacturer's directions by using 12  $\mu\text{g}$  total DNA. For cell sorting, transfections were performed using a construct expressing green fluorescent protein (pEGFP-N1, Clontech) as a marker for cell sorting in combination with PC-1 different constructs (see Fig. 2d). The following day, cells were analysed by FACS Vantage DIVA sorter (Becton Dickinson). Green fluorescent protein-positive cells were sorted, replated in 60-mm dishes containing coverslips and after 36 h cells were analysed by western blotting or challenged by wound healing followed by IF to nuclei and Golgi/microtubule organizing centre as described. Full images of western blottings are shown in Supplementary Fig. S5.

**IP studies and GST pull-down assays.** For immunoblotting, IP study and GST pull-down assay, lysis buffer composed of 150 mM NaCl, 20 mM NaP, 10% glycerol (pH 7.2) supplemented with phosphatase inhibitors (200 mM glycerol phosphate, 200 mM Na orthovanadate and 500 mM Na fluoride), protease inhibitor cocktail (Complete, Roche) and Triton X-100 as indicated.

For GST pull-down assays, the indicated GST-fused PDZ domains of Par3 and HIS-fused C-terminus of PC-1 (aa4132-4303) were expressed in *Escherichia coli* strain BL21. Bacteria were lysed by sonication in 0.1% Triton X-100 lysis buffer and

cleaned by centrifugation. GST-fused protein supernatants were incubated at 4 °C with glutathione beads. Beads were centrifuged, washed and incubated with HIS-fused PC-1 supernatants for 3 h at 4 °C (1:60 in volume of this supernatant was used in immunoblotting as input). After centrifuging and washing the beads, proteins were solubilized in Laemmli buffer and analysed by immunoblotting. Full images of western blottings are shown in Supplementary Fig. S5.

**PAR3 silencing.** Control non-targeting short interfering RNA pool (catalogue number D-001206-13-20) and three short interfering RNA targeting Par3 (Par3#1: 5'-AGACAGACUGGUAGCAGAUUUU-3'; Par3#2: 5'-GUGAAAUUGAGGUCACGCCUUU-3'; and Par3#3: 5'-GUGAAAUUGAGGUCACGCCUU-3'), as well as scramble controls were obtained from Thermo Scientific-Dharmacon. To transiently silence Par3, we used Lipofectamine (Invitrogen) transfection, following the manufacturer's directions.

**Par3-mutant generation and analysis.** Hoxb7Cre mice<sup>27</sup> were bred to mice carrying a mutant allele of Pard3 (ref. 26). Hoxb7Cre;Par3<sup>+/-</sup> males were crossed to females that were homozygous for an allele of Pard3 in which the third coding exon was flanked by loxp sites (*Par3<sup>lox/flox</sup>*). Noon of the day of vaginal plugging was considered embryonic day 0.5. Litters (half females and half males) were collected at various timepoints for mutant analysis and genotyped by PCR. For Cre-recombinase, the following primers were used: Hoxb7Cre: forward 5'-GGT CAC GTG GTC AGA AGA GG-3'; Hoxb7Cre: reverse 5'-CTC ATC ACT CGT TGC ATC GA-3'. Presence of Hoxb7Cre results in a 400-bp product. For Par3, the following primers were used: - 423iF, 5'-AGG CTA GCC TGG GTG ATT TGA GAC C-3'; - 159iR, 5'-TTC CCT GAG GCC TGA CAC TCC AGT C-3'; and + 382iF, 5'-GTC TGT GGG GGT TTT GGG AGA GAG G-3', resulting in products of 371 bp (lox), 292 bp (null) and 265 bp (wt) when resolved on a 3% agarose gel. Mutant embryos (*Hoxb7Cre;Par3<sup>lox/-</sup>*) were compared with littermates either with no Cre (*Par3<sup>-/flox</sup>*) or no null allele (*Hoxb7Cre;Par3<sup>lox/+</sup>*). All animals for these studies were housed, maintained and used according to protocols approved by the Institutional Animal Care and Use Committees at the University of Texas Southwestern Medical Center (animal protocol number 1048-06-01-1).

**Statistical analysis.** Student's *t*-test or one-way analysis of variance was applied to establish differences between means as indicated in the figure legends. Multiple comparisons were carried out using the Bonferroni parameter. Non-parametric Mann-Whitney test was used for the distribution of the angles of migration (Fig. 2b and Supplementary Fig. S3) and for the distribution of cell orientation in the developing tubules (Figs 1e and 6c).

## References

- Costantini, F. Genetic controls and cellular behaviors in branching morphogenesis of the renal collecting system. *WIRE Dev. Biol.* **1**, 693–713 (2012).
- Costantini, F. & Kopan, R. Patterning a complex organ: branching morphogenesis and nephron segmentation in kidney development. *Dev. Cell* **18**, 698–712 (2010).
- Lienkamp, S. S. *et al.* Vertebrate kidney tubules elongate using a planar cell polarity-dependent, rosette-based mechanism of convergent extension. *Nat. Genet.* **44**, 1382–1387 (2012).
- Karner, C. M. *et al.* Wnt9b signaling regulates planar cell polarity and kidney tubule morphogenesis. *Nat. Genet.* **41**, 793–799 (2009).
- Fischer, E. *et al.* Defective planar cell polarity in polycystic kidney disease. *Nat. Genet.* **38**, 21–23 (2006).
- Torres, V. E., Harris, P. C. & Pirson, Y. Autosomal dominant polycystic kidney disease. *Lancet* **369**, 1287–1301 (2007).
- Boletta, A. & Germino, G. G. Role of polycystins in renal tubulogenesis. *Trends Cell Biol.* **13**, 484–492 (2003).
- Nishio, S. *et al.* Loss of oriented cell division does not initiate cyst formation. *J. Am. Soc. Nephrol.* **21**, 295–302 (2009).
- Luyten, A. *et al.* Aberrant regulation of planar cell polarity in polycystic kidney disease. *J. Am. Soc. Nephrol.* **21**, 1521–1532 (2010).
- Wodarczyk, C. *et al.* A novel mouse model reveals that polycystin-1 deficiency in ependyma and choroid plexus results in dysfunctional cilia and hydrocephalus. *PLoS One* **4**, e7137 (2009).
- Boca, M. *et al.* Polycystin-1 induces cell migration by regulating phosphatidylinositol 3-kinase-dependent cytoskeletal rearrangements and GSK3beta-dependent cell cell mechanical adhesion. *Mol. Biol. Cell* **18**, 4050–4061 (2007).
- Etienne-Manneville, S. & Hall, A. Integrin-mediated activation of Cdc42 controls cell polarity in migrating astrocytes through PKCzeta. *Cell* **106**, 489–498 (2001).
- Schmoranzler, J. *et al.* Par3 and dynein associate to regulate local microtubule dynamics and centrosome orientation during migration. *Curr. Biol.* **19**, 1065–1074 (2009).

14. Boletta, A. *et al.* Polycystin-1, the gene product of PKD1, induces resistance to apoptosis and spontaneous tubulogenesis in MDCK cells. *Mol. Cell Biol.* **6**, 1267–1273 (2000).
15. Qian, F. *et al.* PKD1 interacts with PKD2 through a probable coiled-coil domain. *Nat. Genet.* **16**, 179–183 (1997).
16. Qian, F. *et al.* Cleavage of polycystin-1 requires the receptor for egg jelly domain and is disrupted by human autosomal-dominant polycystic kidney disease 1-associated mutations. *Proc. Natl Acad. Sci. USA* **99**, 16981–16986 (2002).
17. Etienne-Manneville, S. & Hall, A. Cell polarity: Par6, aPKC and cytoskeletal crosstalk. *Curr. Opin. Cell Biol.* **15**, 67–72 (2003).
18. Pegtel, D. M. *et al.* The Par-Tiam1 complex controls persistent migration by stabilizing microtubule-dependent front-rear polarity. *Curr. Biol.* **17**, 1623–1634 (2007).
19. Hyodo-Miura, J. *et al.* XGAP, an ArfGAP, is required for polarized localization of PAR proteins and cell polarity in *Xenopus* gastrulation. *Dev. Cell* **11**, 69–79 (2006).
20. Simoes Sde, M. *et al.* Rho-kinase directs Bazooka/Par-3 planar polarity during *Drosophila* axis elongation. *Dev. Cell* **19**, 377–388 (2010).
21. Wodarczyk, C. *et al.* Nephrocystin-1 forms a complex with polycystin-1 via a polyproline motif/SH3 domain interaction and regulates the apoptotic response in mammals. *PLoS One* **5**, e12719 (2010).
22. Aranda, V. *et al.* Par6-aPKC uncouples ErbB2 induced disruption of polarized epithelial organization from proliferation control. *Nat. Cell Biol.* **8**, 1235–1245 (2006).
23. Zallen, J. A. & Wieschaus, E. Patterned gene expression directs bipolar planar polarity in *Drosophila*. *Dev. Cell* **6**, 343–355 (2004).
24. Harris, T. J. & Peifer, M. aPKC controls microtubule organization to balance adherens junction symmetry and planar polarity during development. *Dev. Cell* **12**, 727–738 (2007).
25. Woodward, O. M. *et al.* Identification of a polycystin-1 cleavage product, P100, that regulates store operated Ca entry through interactions with STIM1. *PLoS One* **5**, e12305 (2010).
26. Lin, D. *et al.* A mammalian PAR-3-PAR-6 complex implicated in Cdc42/Rac1 and aPKC signalling and cell polarity. *Nat. Cell Biol.* **2**, 540–547 (2000).
27. Hirose, T. *et al.* PAR3 is essential for cyst-mediated epicardial development by establishing apical cortical domains. *Development* **133**, 1389–1398 (2006).
28. Yu, J., Carroll, T. J. & McMahon, A. P. Sonic hedgehog regulates proliferation and differentiation of mesenchymal cells in the mouse metanephric kidney. *Development* **129**, 5301–5312 (2002).
29. Bertet, C. & Lecuit, T. Planar polarity and short-range polarization in *Drosophila* embryos. *Semin. Cell Dev. Biol.* **20**, 1006–1013 (2009).
30. Yen, W. W. *et al.* PTK7 is essential for polarized cell motility and convergent extension during mouse gastrulation. *Development* **136**, 2039–2048 (2009).
31. Morais-de-Sa, E., Mirouse, V. & St Johnston, D. aPKC phosphorylation of Bazooka defines the apical/lateral border in *Drosophila* epithelial cells. *Cell* **141**, 509–523 (2010).

### Acknowledgements

We are grateful to other members of the lab Boletta, and to L. Feltri, T. Watnick and A. Mondino for help in manuscript structuring/writing; to Dr. T. Pawson for providing Par3 constructs; to T. Hirose for providing the Par3-mutant mice; and to Dr. T. Huber for the Par3 GST-PDZ domains. This work was supported by Telethon-Italy (TCR05007 and GGP12183) to A.B. and by the NIH (1R01DK09505) to T.C. and H.R. A.B. is an Associate Telethon Scientist.

### Author contributions

M.C. designed and performed the experiments, interpreted them, wrote the manuscript. M.B. designed and performed the initial *in-vitro* studies on polarized migration. M.Ch. performed the crossings for the *Pkd1* mutants, collected and analysed data. H.R. performed the crossings for *Par3* mutants, collected and analysed samples. I.R. performed proliferation and apoptosis studies *in vivo* in *Pkd1* mutants and analysed some of the cross-section number of cells in DBA-positive tubules in a blinded manner. G.D. performed the transfection and sorting experiments and analysed data. T.C. supervised the work on *Par3* mutants generation and analysis, and critically read the manuscript. A.B. designed the studies, supervised the work and collaborations, and wrote the manuscript.

### Additional information

**Supplementary Information** accompanies this paper at <http://www.nature.com/naturecommunications>

**Competing financial interests:** The authors declare no competing financial interests.

**Reprints and permission** information is available online at <http://npg.nature.com/reprintsandpermissions/>

**How to cite this article:** Castelli, M. *et al.* Polycystin-1 binds Par3/aPKC and controls convergent extension during renal tubular morphogenesis. *Nat. Commun.* **4**:2658 doi: 10.1038/ncomms3658 (2013).